Progress in Aerospace Sciences 44 (2008) 437–446

Contents lists available at ScienceDirect

Progress in Aerospace Sciences

journal homepage: www.elsevier.com/locate/paerosci

Wall-layer models for large-eddy simulations

Ugo Piomelli

Department of Mechanical and Materials Engineering, Queen's University, Kingston, Ontario, Canada K7L 3N6

A B S T R A C T

The numerical simulation of high Reynolds number flows is hampered by model accuracy if the Reynolds-averaged Navier–Stokes (RANS) equations are used, and by computational cost if direct or large-eddy simulations (LES) that resolve the near-wall layer are employed. The cost of a calculation scales like the Reynolds number to the power 3 for direct numerical simulations, or 2.4 for LES, making the resolution of the wall layer at high Reynolds number infeasible even with the most advanced computers. In LES, an attractive alternative to compute high-*Re* flows is the use of wall-layer models, in which only the outer layer is resolved, while the near-wall region is modeled. Three broad classes of approaches are presently used: bypassing this region altogether using wall functions, solving a separate set of equations in the near-wall region, weakly coupled to the outer flow, or simulating the near-wall region in a global, Reynolds-averaged, sense. These approaches are discussed and their ranges of applicability are highlighted. Various unresolved issues in wall-layer modeling are presented.

Contents

1. Introduction

One main obstacle to the application of large-eddy simulations (LES) to industrial applications is the CPU time required to perform resolved LES of wall-bounded flows. Cost estimates for LES can be found in various Refs. [1–4]. They are based on the consideration that in LES the integral scales of motion must be accurately resolved. In wall-bounded flows the integral scale, away from walls, is proportional to the boundary-layer thickness, δ; a reasonable estimate of the grid spacing in each direction is then $\Delta x_i \simeq \delta/25 - \delta/15$. If one considers a cube of side δ and volume δ^3 as the basic unit, its resolution will require about 800 grid points. In order to simulate a computational domain of dimensions $L_x \times L_y \times L_z$ one needs $N_{c,x} \times N_{c,y} \times N_{c,z}$ unit cubes, with $N_{c,x} = L_x/\delta$ and so on. The number of grid points can then be estimated by multiplying the number of δ^3 cubes by the number of points per cube ($\sim$800). As the Reynolds number *Re* (based on the boundary-layer thickness) is increased, δ decreases, and the number of cubes required to cover the area $L_x \times L_z$ increases (it may be assumed that, in the direction normal to the wall, only a few (2 or 3) boundary-layer thicknesses need to be resolved: in the inviscid region the grid can be coarsened rapidly, so that the number of points required to resolve the potential region is negligible). For boundary-layer flows, in which $\delta \propto Re^{-0.2}$, this results in a number of cubes proportional to $Re^{0.4}$ so that the number of grid points required to resolve the outer layer is

$$(N_x N_y N_z)_{\mathrm{ol}} \propto Re^{0.4}. \tag{1}$$

In the near-wall region,[1] the *Re*-dependence of the resolution is much steeper, since the near-wall eddies that need to be resolved scale with wall units. As the Reynolds number is increased, the physical dimensions of these eddies decrease much more rapidly

[1] We define here the inner layer as the lower 10% of the boundary-layer thickness. For a high-Reynolds number boundary layer, this would include the viscous sublayer, the buffer region and part of the logarithmic layer.

E-mail address: ugo@me.queensu.ca

0376-0421/$ - see front matter © 2008 Elsevier Ltd. All rights reserved.
doi:10.1016/j.paerosci.2008.06.001

than the boundary-layer thickness, resulting in more stringent grid requirements. Assuming that a nested grid system is used, with mesh spacing that increases in all directions as one moves away from the wall, Chapman [1] estimated that the number of points required to resolve the inner layer is

$$(N_x N_y N_z)_{\mathrm{il}} \propto C_{\mathrm{f}} Re^2 \propto Re^{1.8}, \tag{2}$$

where $C_{\mathrm{f}} = 2\tau_{\mathrm{w}}/\rho U^2$ is the skin-friction coefficient, τ_{w} is the wall stress, ρ the fluid density and U a reference velocity (the free-stream velocity in a boundary layer).

To obtain the cost of a calculation one must also consider that the equations of motion must be advanced for several integral time-scales of the flow in order to obtain converged statistics. The time-step is generally determined by a CFL condition, which gives $\Delta t \propto \Delta x/U$ (in attached flows the streamwise direction is the most restrictive from this point of view). Thus, the number of time-steps required to perform a simulation is proportional to the number of grid points in one direction, $N_t \propto Re^{0.2}$ for the outer layer, while $N_t \propto Re^{0.6}$ for the inner layer. The total cost of a calculation, therefore, scales like $Re^{0.6}$ for the outer layer, and like $Re^{2.4}$ if the inner layer is to be resolved.

This cost estimate is shown in Fig. 1, in which the CPU time required to compute a turbulent boundary layer is estimated for three different codes used by the author: a Cartesian code with a staggered, second-order discretization; a co-located finite-volume code suited for body-fitted grids, also second-order in space and time; an unstructured, second-order accurate, finite-volume code. The cost per time-step and grid point was measured on an AMD Opteron processor for a calculation at a given Re, and the scaling laws derived above were used to extend the cost estimate to higher Re. From this figure, one can observe that even at moderate Reynolds numbers ($Re \simeq 10^4$) over 50% of the resources are used to resolve only 10% of the flow. For $Re > 5 \times 10^4$ a vanishing fraction of the grid points is used in the outer layer.

As a consequence of this unfavorable scaling, wall-resolved LES are limited to very moderate Reynolds numbers. Only if massive computational resources (clusters with thousands of processors) are available, calculations at Reynolds numbers of marginal engineering interest ($Re \sim 10^5$) are possible. Resolved LES is clearly not suitable for design, in which substantially more rapid throughput is required to evaluate and compare possible designs within strict time limits, or to study aerodynamic or geophysical flows at $Re = 10^6 - 10^9$.

This limitation was recognized from the earliest applications of LES, and attempt to bypass the inner layer and model its effects in a global sense have been used since the pioneering calculations by Deardorff [5] and Schumann [6]. The basic consideration, in simulations in which the inner layer is modeled (wall-modeled LES, or WMLES), is that the grid near the wall is too coarse to resolve the eddies that contribute to the momentum transport. If the mixing due to the near-wall eddies is not computed when no-slip conditions are applied, an incorrect velocity profile results, and under-prediction of the wall stress. Therefore, one must model the transport of momentum by the inner-layer scales either implicitly, by relating the outer-layer velocity to the wall stress through an assumed velocity profile, or explicitly, by parameterizing their effect in the Reynolds-averaged sense. The critical assumption that must be made is that the near-wall grid is so coarse that it contains a very large ($\to \infty$) number of near-wall eddies, and that the time-step is much larger than their time-scale, so that the filtering operation becomes equivalent to a Reynolds average.

Deardorff [5] and Schumann [6] bypassed the inner layer by using approximate boundary conditions similar to the wall functions applied in Reynolds-averaged Navier–Stokes (RANS) simulations with turbulence models. These boundary conditions assume the existence of an equilibrium layer in which the stress is constant. This results in the existence of a logarithmic layer that can be used to relate the velocity in the outer layer to the wall stress.

The development of more powerful computers resulted in wall-resolved LES of wall-bounded flows at low or moderate Reynolds numbers (for instance [7]), which allowed more detailed studies of the turbulence physics. Approximate boundary conditions, however, remained in widespread use in environmental and geophysical flows. In these flows the geometry is generally quite simple, and the Reynolds number extremely high, so that the equilibrium layer assumption holds in most situations; corrections can be made for buoyancy, roughness and other effects common in these applications.

In engineering flows the use of approximate boundary conditions based on the equilibrium-stress layer approximation is less applicable. In the presence of strong favorable or adverse pressure gradients, in separated flows or in flows in which the mean velocity is highly three-dimensional, the assumption of the existence of a logarithmic law does not hold. This prompted first the derivation of corrections for models based on the logarithmic

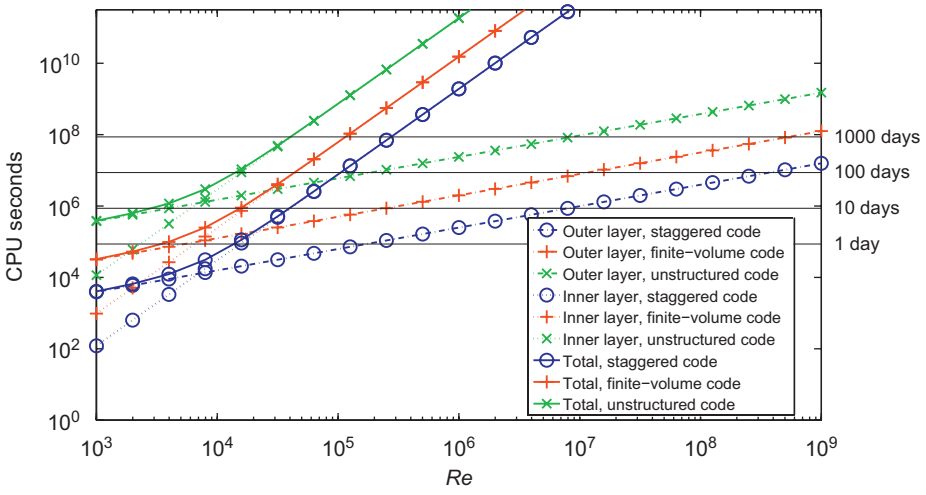

Fig. 1. Cost, in CPU seconds, of the LES of flat-plate boundary-layer flow. The calculations were performed on an AMD Opteron, using two in-house codes and an open-source unstructured one. Actual mileage may vary.

law [8–10], and then the development of hybrid models in which simpler transport equations are solved in the inner layer, weakly or strongly coupled to the outer-flow LES.

The two-layer model (TLM), originally proposed by Balaras and coworkers [11,12], has weak coupling between the inner and outer layers. A fine one-dimensional grid is embedded between the first grid point and the wall, and a simplified set of equations (generally, the Reynolds-averaged turbulent boundary-layer equations) is solved in the embedded mesh. The outer-layer LES provide the boundary condition for the inner layer, whereas the inner-layer calculation provides the wall stress required by the LES. Cabot [13,14] and Cabot and Moin [15] explored various features of this model, which was successfully used also by Wang and Moin [10] in the simulation of a trailing-edge flow. A similar approach, based on the two-layer simulation (TLS) method [16,17] was applied by Gungor and Menon [18].

The use of hybrid simulations in which the RANS equations are used in the inner layer, while the filtered Navier–Stokes equations are solved in the outer layer, has become increasingly popular in the past few years. Several strategies can be used to switch between one model and the other, such as changing the length scale in the model from a RANS mixing length to one related to the grid size, or using a blending function to merge the SGS and RANS eddy viscosities.

The direct modification of the length scale is used in the detached eddy simulation [19] approach, and was employed by Nikitin et al. [20] for the simulation of turbulent channel flow at Reynolds numbers (based on the friction velocity $u_\tau = (\tau_w/\rho)^{1/2}$ and channel half-height) up to 80,000. The model was able to sustain turbulence, but the logarithmic layer in the LES region was displaced upwards, resulting in a 15% under-prediction of C_f. Baggett [21] attributed this error (known as "logarithmic law mismatch", LLM) to the delayed generation of resolved eddies in the interface region between the RANS and LES zones. Piomelli et al. [22] and Keating and Piomelli [23] found that the addition of stochastic forcing in the interface region accelerated the generation of resolved eddies, leading to more accurate results. Radhakrishnan et al. [24], however, observed that in cases in which mean-flow perturbations (adverse pressure gradients, separation) create more unstable flow conditions, accurate results can be obtained even without the stochastic forcing.

Several researchers have used hybrid RANS/LES schemes in which a blending function is used to bridge the RANS and LES zones. Hamba [25,26], performed channel flow simulation using various hybrid RANS/LES models and suggested a method to improve the mean velocity prediction through additional filtering. He observed that the filter width in the RANS region is larger than that in the LES region at the RANS/LES interface. To remove this inconsistency, he defined two wall-normal velocity components at the interface; one based on the LES filter width and another based on the RANS filter width. The RANS velocity is obtained from the LES one by additional filtering. This method introduces source terms in both continuity and momentum equation and provides forcing at the interface region whose effects are similar to the forcing used in Refs. [22,23].

Temmerman et al. [27] calculated channel flow and a separated flow in a channel constricted by a curved hill using hybrid RANS/LES method. In their hybrid method, the eddy viscosity in the RANS region is defined by $C_\mu k_{mod}^{1/2} l_\mu$, where C_μ is a constant, k_{mod} is the modeled turbulent kinetic energy and l_μ is the length scale, which is either explicitly prescribed or obtained by solving an additional transport equation. They obtained the constant, C_μ, by equating the RANS eddy viscosity to the LES eddy viscosity at the interface. They were able to remove the shift in the mean velocity, when they used the C_μ value obtained instantaneously at every point rather than using an averaged value along the homogeneous direction. Use of spatially and temporally varying C_μ also results in the introduction of additional unsteadiness near the RANS/LES interface.

Davidson and Peng [28] calculated channel flow and separated flow past a hill using a hybrid RANS/LES method based on $k-\omega$ model in the RANS region, and the one-equation subgrid-scale turbulent kinetic energy model of Yoshizawa [29] in the LES region. They also observed the LLM in the channel flow, and obtained better results in the separated flow, which they attributed to the enhanced convective and diffusive transport across the interface in the latter flow. Davidson and Dahlstrom [30] computed channel flow and flow past a asymmetric plane diffuser using a hybrid RANS/LES method with a one-equation model for turbulent kinetic energy. In their simulation, forcing was provided at the interface by adding a source term to the three momentum equations based on velocity fluctuations taken from a DNS database. With a carefully chosen coefficient for the source term, they were able to remove the LLM in the channel flow.

Edwards and coworkers [31–33] performed hybrid simulations of supersonic flows using Menter's SST model [34] and a variety of blending functions. They find that it is important to use turbulence properties (rather than grid-related quantities) in the definition of the blending function; in Ref. [33] they obtain accurate results using a blending function that uses the Taylor microscale as turbulence length scale. They observe, however, that blending functions based on modeled quantities may exhibit problem-specific responses, which can sometimes lead to non-unique solutions (J.R. Edwards, personal communication, 2008).

Even this brief and incomplete summary of existing approaches for WMLES should alert the reader to the many challenges that this technique, not surprisingly, faces. Given the complexities of the flow in the inner layer, and its importance in establishing the production cycle [35], one cannot expect that modeling its effects on the outer flow may be easy or painless, or that equal accuracy can be achieved compared with wall-resolved calculations. It is, nonetheless, critical to develop reasonably accurate wall-layer models, and also to estimate the errors that can be expected from WMLES. In the following, the three general techniques discussed above will be described in more detail, and the challenges and achievements of each will be presented and discussed.

2. Equilibrium-stress models

The assumption that a constant-stress layer exists near the wall implies that the velocity at the first point in the outer layer satisfies a logarithmic profile [36]:

$$U_{ol}^+ = \frac{U_{ol}}{u_\tau} = \frac{1}{\kappa}\log\frac{y_{ol}u_\tau}{\nu} + B, \tag{3}$$

where the subscript ol indicates the first grid point in the outer layer, and $U_{ol} = \langle\overline{u}_{ol}\rangle_{xz}$ is the velocity at the first outer-layer point averaged over an xz-plane.[2] The von Kàrmàn constant κ is generally taken to be 0.41 [36], and $B \simeq 5.0-5.5$. The logarithmic law (3) can be matched to a linear law $U_{ol}^+ = y_{ol}^+$ for $y_{ol}^+ < 11$ to account forlow-Reynolds number effects.

This relationship can be used in a number of ways. Deardorff [5] imposed that (3) be satisfied in the mean for $\overline{u}$, and required that the second derivatives of $\overline{u}$ and $\overline{u}$ in y be locally isotropic with respect to the second derivative in z and x, respectively. Schumann [6] obtained the mean stress from the global momentum balance

[2] In the following, x will be the mean-flow direction, y the direction normal to the wall, and z the spanwise direction. u, v and w are the respective velocity components. An overline indicates a filtered variable.

($\langle\tau_w\rangle$ is balanced by the imposed pressure gradient in a channel or duct flow) and then used the following boundary conditions for the streamwise and spanwise components of the wall stress:

$$\tau_{w,x}(x,z,t) = \left[\frac{\langle\tau_w\rangle_{xz}}{U_{ol}}\right]\overline{u}(x,y_{ol},z,t), \tag{4}$$

$$\tau_{w,z}(x,z,t) = \left[\frac{\langle\tau_w\rangle_{xz}}{U_{ol}}\right]\overline{w}(x,y_{ol},z,t), \tag{5}$$

where the dependence of U_{ol} and $\langle\tau_w\rangle$ on time is omitted. Grötzbach [37] applied similar conditions but obtained the wall stress by solving (3) for u_τ.

Piomelli et al. [8] applied conditions similar to (4) and (5). However, to take into account the inclination of the elongated structures in the near-wall region, they required that the wall stress be correlated to the instantaneous velocity some distance Δ_s downstream of the point where the wall stress is required. In addition to the streamwise shift, Marusic et al. [38] suggested separating the mean wall stress from its fluctuating part, which can be multiplied by a constant to match the wall-stress fluctuations better. The model they propose (which will be referred to as "MKP model") replaces (4) and (5) with

$$\tau_{w,x}(x,z,t) = \langle\tau_w\rangle_{xz} + \alpha_\tau u_\tau[\overline{u}(x+\Delta_s,y_{ol},z,t) - U_{ol}], \tag{6}$$

$$\tau_{w,z}(x,z,t) = \alpha_\tau u_\tau \overline{w}(x+\Delta_s,y_{ol},z,t). \tag{7}$$

Here, α_τ is a constant (the value 0.10 was suggested in Ref. [38] to match the spectrum of τ_w given by (6) with the experimental one).

Several simple modifications of the standard approximate boundary conditions are possible. Mason and Callen [39] applied the logarithmic law instantaneously (an approximation whose accuracy depends critically on the dimensions of the grid, which needs to be exceptionally large, in wall units). Wu and Squires [40] calculated the flow over a bump and obtained u_τ from a separate RANS calculation. Hoffman and Benocci [9] and Wang [41] modified the logarithmic law by including the effects of local acceleration and pressure gradients. Werner and Wengle [42] replaced the logarithmic law with a power law. Other modifications can be made to include the effects of buoyancy (see for instance [43]) or roughness.

The assumptions underlying the approximate boundary conditions discussed in this section are quite strong, and when turbulence is not in equilibrium these models may fail catastrophically. Balaras et al. [12], for instance, report that the model diverged when it was applied to a rotating channel flow, in which the turbulence is damped on one side of the channel and amplified on the other. More commonly, these models fail in flows with shallow separation, or with strong pressure gradients.

Fig. 2, for instance, shows the mean streamlines and contours of resolved Reynolds shear stress $\langle u'v'\rangle$ for three calculations of the flow over a contoured ramp. More detail on these calculations, and more complete comparisons with experimental data can be found in [24,44,45]. The geometry is that used by Song and Eaton [46] for their experiments: the height of the ramp is comparable to the boundary-layer thickness, and shallow separation is observed at 70–75% of the ramp length. Three models are compared: LES that use the logarithmic law as an approximate boundary condition, and two hybrid calculations that use the DES approach with the Spalart–Allmaras (SA) [47] eddy-viscosity model, which will be described later. The model based on the logarithmic law does not predict the separation at all. That is not surprising, since the grid is so coarse that most of the recirculation occurs below the first grid point. The flow prediction in the immediate vicinity of the ramp trailing edge is significantly wrong; one can observe also how the instability in the separated shear layer amplifies the eddy generation there in the hybrid calculations, resulting in elevated levels of Reynolds shear stress that are not observed in the logarithmic-law model.

In attached flows, even in the presence of fluid-dynamical non-equilibrium, the logarithmic-law approximate boundary condition may give more accurate results. Fig. 3 shows the mean velocity field in an oscillating boundary layer [48]. The freestream is subjected to a sinusoidal oscillation, $U_\infty = U_{om}\sin\omega t$. The relevant dimensionless number for this flow is the Reynolds number based on the Stokes-layer thickness, $\delta_s = (2\nu/\omega)^{1/2}$ and on the freestream velocity oscillation amplitude, U_{om}. For this case, $Re_\delta = 3500$, resulting in a flow with fairly long period, turbulent through the entire cycle. Two calculations that use the logarithmic-law boundary condition (one in its standard form, the other with the MKP modification) and the Lagrangian dynamic eddy-viscosity (LDEV) model [49] are compared with a hybrid RANS/LES that uses the SA model. Here, $\phi = \omega t$ is the phase angle. In this case we observe much better agreement between the simulations that apply the logarithmic law and the experimental data [50]. The hybrid calculation predicts a very high eddy viscosity in the near-wall region, and results in excessive mixing, with a very flat outer-layer profile through most of the cycle, and a high velocity in the near-wall region near flow reversal ($\phi = 0^\circ$). The two calculations that use the LDEV model give essentially the same result (the curves are indistinguishable at least during the first three phases).

Instantaneous picture of the flow for a simulation with logarithmic-law approximate boundary conditions is shown in Fig. 4. We show isosurfaces of the second invariant of the velocity gradient tensor, Q:

$$Q = -\tfrac{1}{2}(\overline{\Omega}_{ij}\overline{\Omega}_{ij} - \overline{S}_{ij}\overline{S}_{ij}), \tag{8}$$

which has been shown to be effective in highlighting coherent vortical structures [51,52]. We observe the damping of turbulent eddies during the acceleration phase, followed by their rapid regeneration as the freestream velocity becomes approximately constant. During the deceleration phase, a realistic distribution of hairpin vortices can be seen, with a predominance of "heads" [53], as expected in the outer layer of a wall-bounded flow.

3. Zonal approaches

The logarithmic law implies an implicit integration of the averaged boundary-layer equations from the first grid point to the wall, under the assumption of constant stress, with a mixing-length model to parameterize turbulent transport. Hoffman and Benocci [9] tried to incorporate the effect of pressure gradient and local acceleration, still within the framework of an integral formulation. Balaras and Benocci [11], on the other hand, solved the turbulent boundary-layer equations on an embedded grid between the first grid point (which should be placed at the edge of the inner layer) and the wall:

$$\frac{\partial\overline{u}_i}{\partial t} = -\frac{\partial}{\partial x_j}\overline{u}_i\overline{u}_j - \frac{\partial P_e}{\partial x_i} + \frac{\partial}{\partial x_j}\left[(\nu+\nu_T)\frac{\partial\overline{u}_i}{\partial x_j}\right] \quad \text{for } i=1,3, \tag{9}$$

$$\overline{u}_2 = -\int_0^y\left(\frac{\partial\overline{u}_1}{\partial x_1} + \frac{\partial\overline{u}_3}{\partial x_3}\right)\mathrm{d}y, \tag{10}$$

here, $\partial P_e/\partial x_i$ is the pressure gradient at the first point in the outer layer, which is imposed through the embedded grid, and ν_T is the eddy viscosity (given by a simple Prandtl mixing length in [11]).

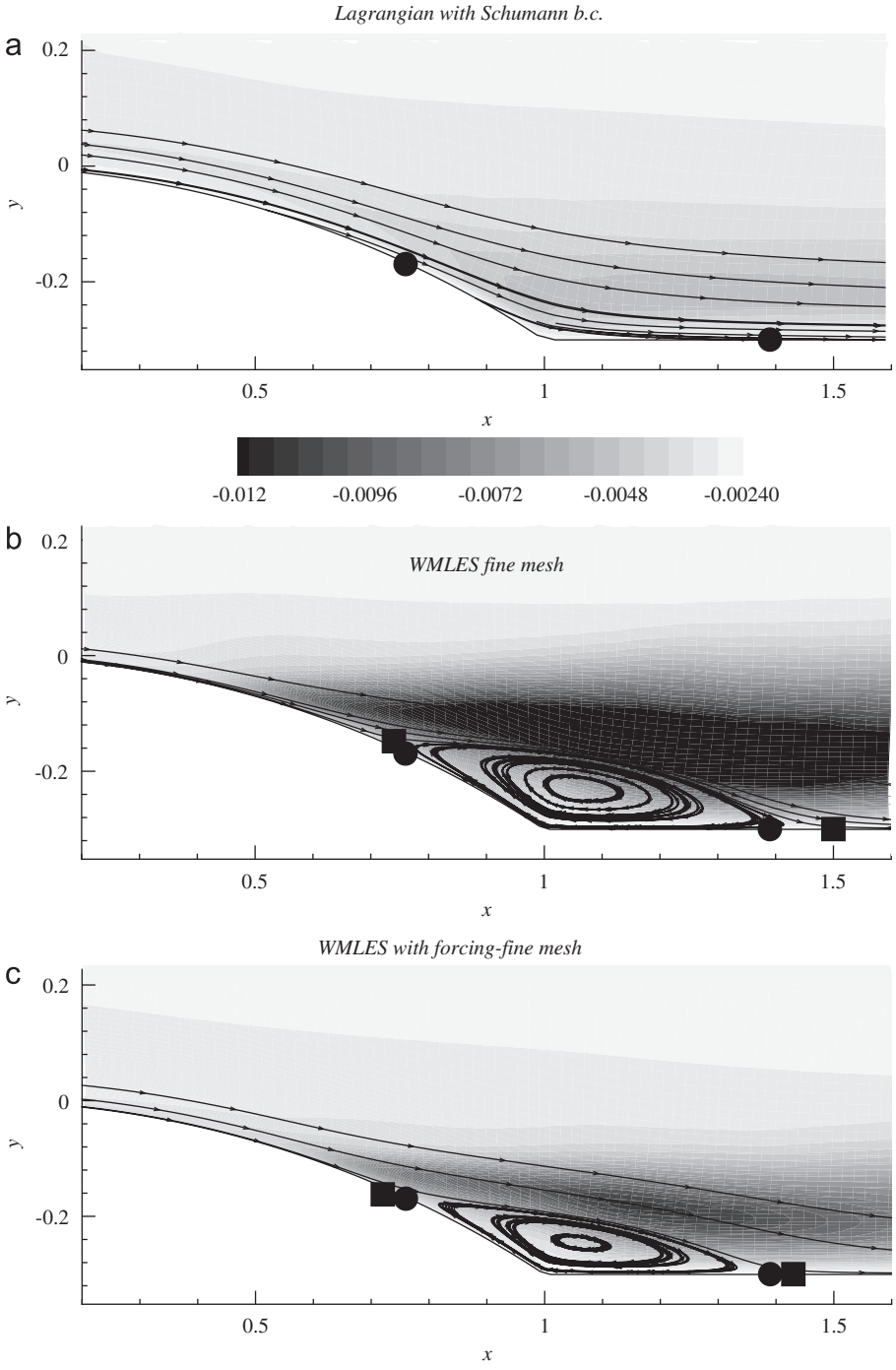

Fig. 2. Streamlines and contours of $\langle u'v' \rangle$ in the separated-flow zone of a contoured ramp. (a) Logarithmic-law boundary condition; (b) SA WMLES without stochastic forcing; (c) SA WMLES with stochastic forcing. The solid dots represent the experimentally measured separation and reattachment points, the squares the computed ones.

Balaras et al. [12] applied this approach to rotating channel flow and flow in a square duct, and obtained improved agreement with the experimental data, compared with the simple logarithmic law. Cabot [13,14] examined the importance of the terms on the right-hand-side of (9) and found that, in plane channel flow, imposing the balance between imposed pressure gradient and viscous plus turbulent diffusion (i.e., imposing an instantaneous logarithmic law) is sufficient. In a backward-facing step, on the other hand, all terms in (9) are important.

More recent applications of the TLM include the work of Diurno et al. [55], who also computed the flow in a backward-facing step using a SA model for ν_T, which improved the agreement with the data. Wang and Moin [10] used the TLM for the computation of acoustic emission from a trailing-edge geometry with good success. They demonstrated that the RANS-type eddy viscosity must be reduced to account for the resolved fluctuations inside the inner layer. The improvement in the results can be seen in Fig. 5, in which the skin-friction coefficient is compared for a calculation that uses the TLM with $\kappa = 0.4$ (κ is the proportionality constant in the mixing-length eddy viscosity model) with one in which the constant is determined dynamically.

Gungor and Menon [18] performed calculations of plane channel flow and flow over an axisymmetric hill using the TLS

method, in which the small-scale velocity is simulated in each grid cell using a reduced-order form of the governing equations for the small scales: the equations are solved along three one-dimensional lines aligned with the coordinate axes [16,17]. While the agreement with experimental data is good for the plane channel flow, the velocity is over-predicted in the hill simulations, perhaps due to excessively coarse outer-layer resolution.

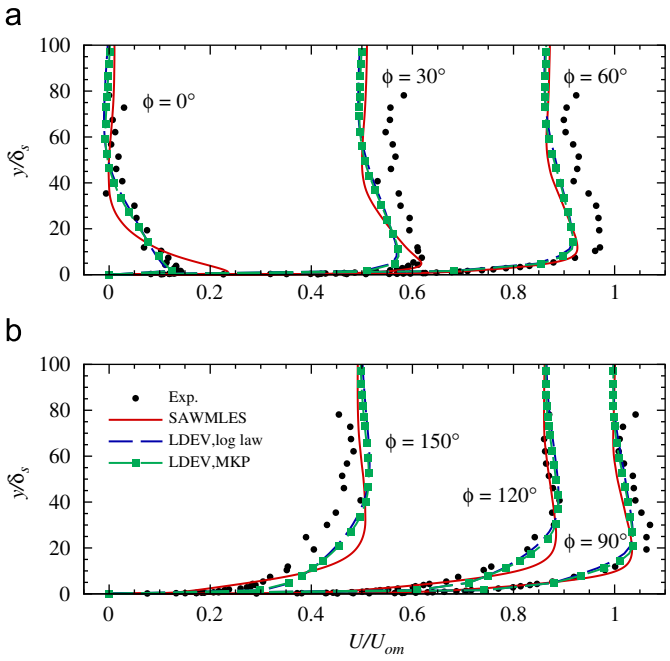

Fig. 3. Mean velocity profiles, oscillating boundary layer. (a) $\phi = 0^\circ$, 30° and 60°; (b) $\phi = 90^\circ$, 120° and 150°.

4. Hybrid RANS/LES methods

Much work has recently gone into developing hybrid methods, in which the RANS equations are solved in the inner layer, while the filtered Reynolds-averaged equations are solved away from the wall. The main issue that affects such hybrid RANS/LES methods is the disparity of scales between the LES and RANS regions. In the wall-layer modeling techniques described so far, the outer layer imposes its scales on the inner one, which therefore contains eddies as small as the filter size. In hybrid methods, on the other hand, the inner layer has its own time- and

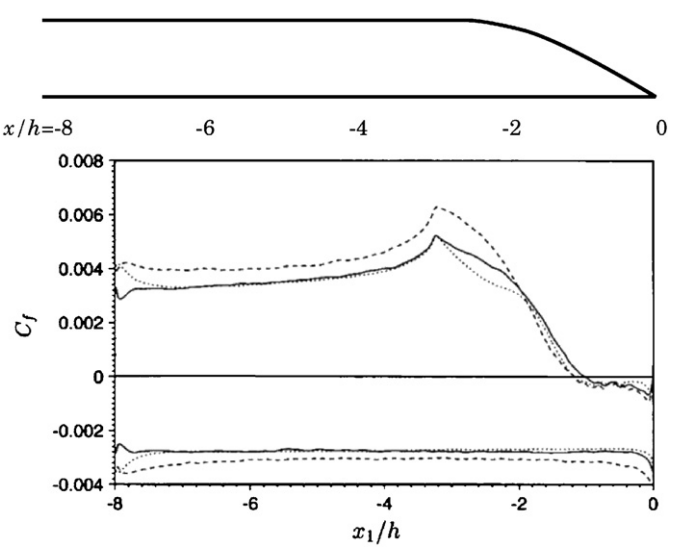

Fig. 5. Distribution of skin-friction coefficient in the trailing-edge computed using LES with the turbulent boundary layer equation wall model. --- $\kappa = 0.4$; — dynamic κ; ..... resolved LES [54]. Reused with permission from M. Wang [10]. Copyright 2002, American Institute of Physics.

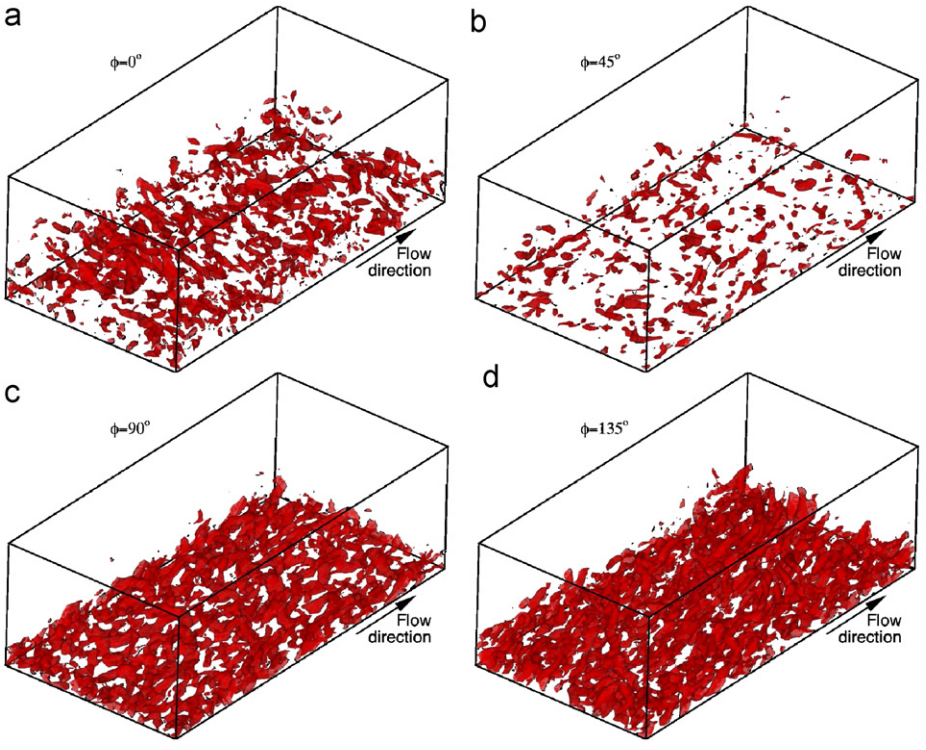

Fig. 4. Oscillating boundary-layer flow. Instantaneous isosurfaces of $Q = 1$ [Q is defined in Eq. (8)]. (a) $\phi = 0^\circ$; (b) $\phi = 45^\circ$; (c) $\phi = 90^\circ$; (d) $\phi = 135^\circ$.

length-scales (determined by the unsteady RANS equations applied there) which are generally much larger than those of the outer-layer eddies. This is illustrated in Fig. 6 (from Ref. [22]), which shows time-histories of the velocity at several locations in a plane channel. The calculation used the hybrid WMLES based on the SA [47] model, and the nominal interface between the RANS and LES regions was at $y^+ = 225$ ($y/\delta \simeq 0.05$). First, one can observe that the flow in the RANS region is not steady, but that low frequency fluctuations can be observed (time in the figure is normalized by u_τ and δ, so that the observed period, about 0.3–0.5 units, is of the order of the large-eddy turnover time). At $y^+ = 421$ (well above the RANS/LES interface), higher frequencies begin to appear, but the dominant time-scale is still the one characteristic of the inner-layer flow, i.e., the time-scale imposed by the RANS model. Only very far from the wall one observes the high-frequency fluctuations that one expects in such flows. Similar observations can be made in terms of length scales: the eddies immediately above the RANS/LES interface maintain the length scales characteristic of the RANS zone, and only very far from the wall the small eddies appear that are capable of supporting the Reynolds stress in the LES region.

The effects of the lack of resolved eddies in the interface region can be seen very well in Fig. 7(a), which shows the profiles of the modeled and resolved stress in a SA-WMLES of turbulent plane channel flow at $Re_\tau = 5000$. The modeled stress is significantly larger than the resolved one even a significant distance above the nominal interface between RANS and LES. The location where the modeled and resolved stresses are equal can be used to define the extent of an effective transition region, in which eddies are generated that are capable to resolve the Reynolds shear stress. Only beyond this transition region the eddy content of the calculation is sufficient to support most of the Reynolds shear stress.

As discussed by Baggett [21] the lack of resolved eddies in the interface region results in the LLM, which can be observed in the velocity profiles shown in Fig. 8. Since the total shear stress, in the plane channel, is only a function of distance from the wall (and is determined by the global momentum balance), the decrease in the eddy viscosity that occurs beyond the RANS/LES nominal interface, if not accompanied by a corresponding increase of the resolved Reynolds stress, must result in an increase in the mean velocity gradient. This "DES buffer layer" bridges an inner region, in which the logarithmic layer has the correct slope and intercept, with an outer layer in which the slope is correct, but the intercept is shifted upwards.

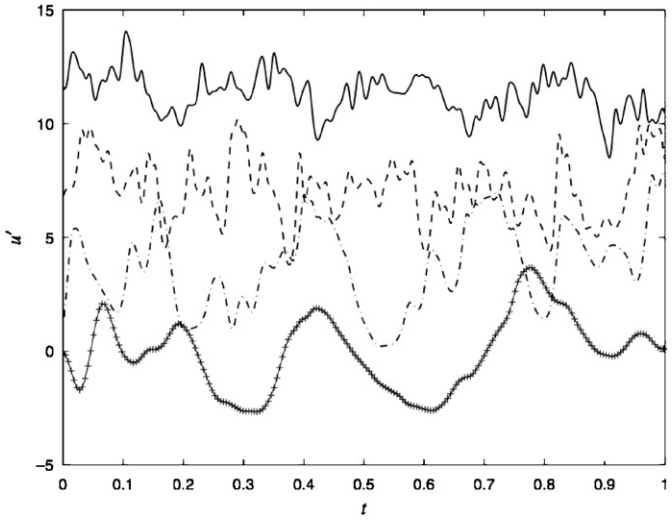

Fig. 6. Time-history of the velocity at various heights above the wall for a SA-WMLES of plane channel flow at $Re_\tau = 5000$. + $y^+ = 18$; –·– $y^+ = 421$; - - - $y^+ = 1107$; — $y^+ = 3124$. Reused with permission from U. Piomelli [22]. Copyright 2003, Elsevier Science Inc.

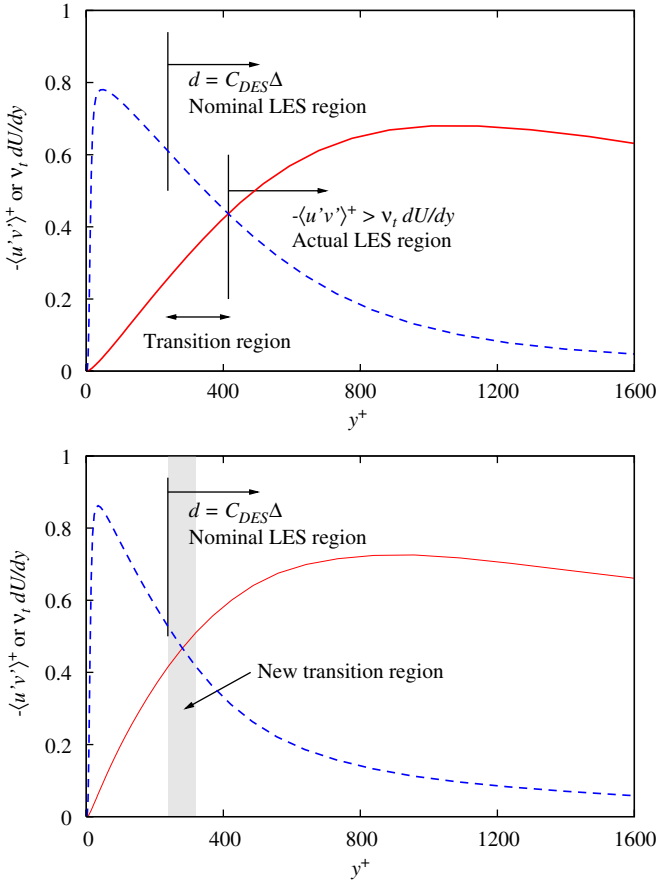

Fig. 7. Profiles of modeled and resolved shear stress after dynamic stochastic forcing. Turbulent channel flow at $Re_\tau = 5000$. — Resolved shear stress, $-\langle u'v'\rangle$; - - - modeled shear stress, $\langle \nu_t \rangle\, dU/dy$. (a) SA-WMLES with no stochastic forcing. (b) SA-WMLES with stochastic forcing. Reused with permission from U. Piomelli [23]. Copyright 2006, Taylor & Francis.

The LLM is a feature common to most hybrid RANS/LES schemes. In the framework of SA-based WMLES it was observed by Nikitin et al. [20], discussed by Baggett [21], Piomelli et al. [22] and Keating and Piomelli [23]. Hamba [25,26] observed it in WMLES that used a $k-\varepsilon$ model; Temmerman et al. [27] and Tessicini et al. [56] also observed it in hybrid calculations that use a $k-l$ or a $k-\varepsilon$ model. These researchers spend a considerable effort trying to reduce or remove the LLM by various methods, and achieve some measure of success when they introduce artificial fluctuations in the interface region, which are then amplified by the flow itself. The calculations by Keating and Piomelli [23], which use stochastic forcing at the RANS/LES interface, illustrate this phenomenon: the resolved stresses are significantly enhanced near the RANS/LES interface (Fig. 7(b)), resulting in a much reduced transition region. Fig. 8 shows how the LLM is reduced for a range of Reynolds numbers. Improved results were obtained also in the calculations of the separated flow over a contoured ramp [44]: Fig. 2 shows both better agreement of the separation and reattachment points with the experimental measurements, and also lower levels of $\langle u'v'\rangle$ stresses, again in good agreement with the experimental data of Song and Eaton [46]. Accelerating artificially the development of the eddies capable of supporting the Reynolds stress appears to be an effective method of decreasing the extent of the transition region.

Travin et al. [57] and Shur et al. [58] followed a different approach: they developed a special blending function for an SA-based WMLES, which decreases the viscosity significantly in the interface region (Fig. 9). In a standard SA-WMLES the eddy viscosity generally increases monotonically, and does not exhibit the dip shown in the figure. Also notice that the minimum eddy viscosity occurs around the interface between the inner and outer layer, i.e., at a distance approximately equal to $\delta/10$ from the wall; depending on the Reynolds number, this translates into the beginning or the middle of the logarithmic region. The eddy-viscosity decrease makes the flow in the RANS/LES transition region less stable, and allows any flow perturbation to be amplified more rapidly. Their calculations show very good agreement with the data in a variety of flows, with a complete removal of the LLM.

In summary, hybrid RANS/LES methods seem to be most effective in flow conditions that facilitate the rapid amplification of any instability, whether due to numerical or natural causes. Separation, concave curvature and adverse pressure gradients have this effect. In such cases, the eddy generation at the RANS/LES interface is greatly increased, and accurate results can be obtained (see for instance the discussion in [24]). These models are least accurate in attached, thin shear layers, where the instability mechanisms are comparatively weak; in addition to the LLM discussed before, other errors can be observed: in the oscillating boundary-layer flow discussed before (Fig. 3), for instance, the SA-WMLES predicts excessive levels of eddy viscosity in the near-wall region. Consequently, the response of the inner layer to the freestream oscillation is predicted incorrectly; the high eddy viscosity leads to excessive mixing in the outer flow, and the inner-layer response is delayed compared to the experimental data (and the models based on the logarithmic law).

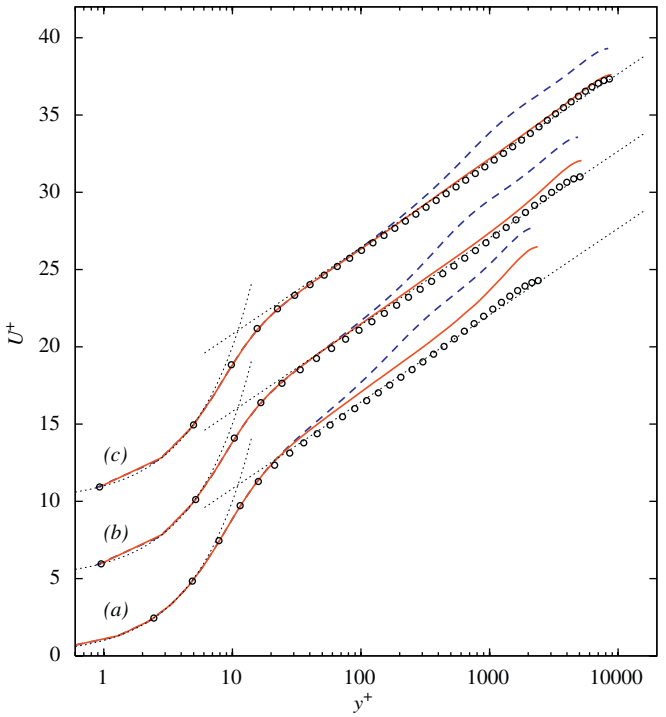

Fig. 8. Turbulent channel flow: mean velocity profiles in wall units. (a) $Re_\tau = 2300$, (b) $Re_\tau = 5000$, (c) $Re_\tau = 8000$. --- SA-WMLES with no stochastic forcing; — SA-WMLES with stochastic forcing; ○, SA-RANS. Profiles are shifted by 5 units in y for clarity. Reused with permission from Piomelli [23]. Copyright 2006, Taylor & Francis.

It should be noted here that Germano [59] derived rigorously the governing equations obtained when a hybrid RANS/LES filter is applied to the Navier–Stokes equations, and showed that additional terms appear both in the conservation equations of mass and momentum, and in the definition of the unclosed stress. These additional terms have the form of scale-similar models, with products of differences between filtered and Reynolds-averaged velocities, and are most significant in the interface region. They can conceivably act to enrich the eddy content in the interface region, with the same effect as the forcing terms that have been used successfully by other researchers. Early applications of this approach [60–62] show that the inclusion of the hybrid terms is beneficial, and may relieve some of the empiricism required by many of the other methods.

5. Concluding remarks

In this article, the current status of wall-layer modeling has been briefly reviewed. Three classes of models are described: equilibrium laws based on the logarithmic law (or on some similar assumed velocity profile); zonal models, in which the turbulent boundary-layer equations are solved, weakly coupled to the outer-layer LES; hybrid methods in which the model changes from a RANS-based turbulent model near the wall to LES mode in the outer layer.

Equilibrium laws are the least expensive model, in terms of computational requirements. The cost of simulations of this kind scales like the cost of the outer layer, $Re^{0.6}$. Zonal models require between 10% and 20% more CPU time for the solution of the boundary-layer equations, and significantly more memory. The cost of hybrid RANS/LES methods is higher, since the wall-normal direction must be well resolved (the SA model, for instance,

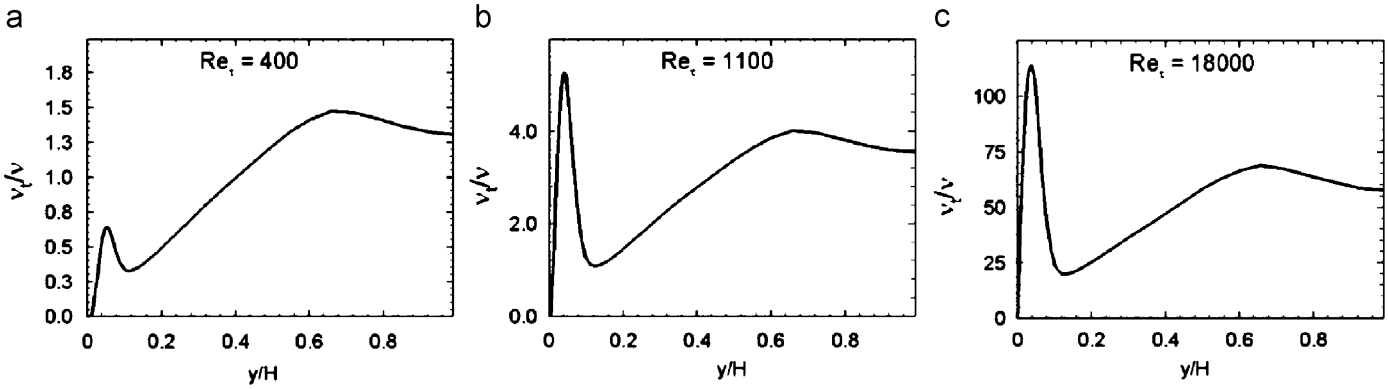

Fig. 9. Profiles of IDDES eddy viscosity normalized by the molecular viscosity in developed channel flow at different Re_τ. Reused with permission from M. Kh. Strelets.

requires that the first point be at $y^+ \simeq 1$), so that the number of grid points in the wall-normal direction is proportional to $\log Re$, resulting in a cost that scales approximately like $Re^{0.6} \log Re$.

It is unreasonable to expect that WMLES may ever be as accurate as resolved LES: at least in equilibrium flows, the inner layer is the region where most of the production takes place, and the eddies are created that grow and are advected into the outer layer, affecting the momentum transport there too. It may be overly optimistic to hold the same accuracy standards for simulations that include such important physical phenomena, and those that bypass them. Despite this intrinsic shortcoming, WMLES are able to predict with reasonable accuracy a wide variety of flows; in many cases the physics of the outer layer are reproduced well, despite the fact that the inner layer is bypassed (see, for instance, the relaminarization–retransition sequence illustrated in Fig. 4), as long as the grid is sufficiently fine to resolve the outer-flow integral scale.

In WMLES the resolution of the outer layer is, in fact, an often overlooked issue. Bypassing the wall layer is sometimes viewed as justification to use excessively coarse grids everywhere; however, many of the simulations shown here forcefully demonstrate that, unless the integral scale in the outer layer is resolved well, uniformly accurate results cannot be obtained. Several of the author's own calculations (see, for instance Refs. [23,24,48]) show how grid sizes greater than $\delta/15$ do not result in grid-independent results, and often give incorrect prediction of the Reynolds stresses.

Another issue that is often overlooked is the subgrid-scale modeling error in the outer layer in the vicinity of the wall. This is a region in which the flow integral scale is proportional to the distance from the wall, and is necessarily smaller than (or, at best, comparable to) the grid size. Nicoud et al. [63] used suboptimal control theory to supply a wall stress that forced the outer LES to the desired mean velocity profile. With this method the approximate boundary condition compensates for subgrid-scale modeling and numerical errors, and obtained improved results over standard approximate boundary conditions. This approach, however, is infeasible as a predictive tool, since it requires the solution to be known *a priori* to generate the desired cost function. Corrections to the subgrid-scale stresses near the wall (see, for instance [64]) may be a more realistic technique to improve the model accuracy near the wall. Hybrid methods do not suffer from this constraint, since the RANS model is used to parameterize all the scales of motion in the near-wall region, and the LES zone is restricted to the region of the flow where the grid size is sufficiently smaller than the integral scales to ensure its proper resolution.

At this point, there is no single method that is clearly superior to the others. Equilibrium laws give reasonably accurate results in attached flows, with mild pressure gradients and curvature. Zonal models have had some success in flows in which the outer layer drives the inner one, less so when the perturbation is propagated from the wall outwards. Hybrid methods are most accurate when the mean flow has some destabilizing perturbation that accelerates the generation of Reynolds-stress supporting eddies. Although the effects of wall roughness (a very important feature in environmental and oceanographic flows) can be included in hybrid RANS/LES models, no study of the accuracy of roughness corrections for WMLES is known to the author. Equilibrium laws, on the other hand, can include roughness corrections very easily through modifications of the logarithmic law.

The review paper by Piomelli and Balaras [4] final statement that "one may hope that the next five years or so may bring substantial advancement in this area as well" has been revealed to be perhaps excessively sanguine. Despite the increased attention to the problem, no universally accepted model has appeared. There is, however, a better understanding of the limitations and applicability of WMLES, and a more complete vision of the interplay between numerical errors, subgrid-scale modeling errors, and inaccuracies of the wall-layer model. There is still reason to believe that more general models may be forthcoming for the calculation of high-Reynolds number flows by LES.

Acknowledgments

The author's research on wall-layer models has been supported for several years by the Office of Naval Research, under a sequence of grants monitored by Drs. L.P. Purtell and R.D. Joslin. More recent work on the application of LES to geophysical flows has been supported by the National Science Foundation, under Grant no. OCE0452380, monitored by Dr. E. Itsweire.

References

[1] Chapman DR. Computational aerodynamics development and outlook. AIAA J 1979;17:1293–313.
[2] Reynolds WC. The potential and limitations of direct and large eddy simulations. In: Lumley JL, editor. Whither turbulence? Turbulence at the crossroads. Lecture notes in physics, vol. 357. Berlin: Springer; 1990. p. 313–43.
[3] Spalart PR. Strategies for turbulence modelling and simulations. Int J Heat Fluid Flow 2000;21:252–63.
[4] Piomelli U, Balaras E. Wall-layer models for large-eddy simulations. Annu Rev Fluid Mech 2002;34:349–74.
[5] Deardorff JW. A numerical study of three-dimensional turbulent channel flow at large Reynolds numbers. J Fluid Mech 1970;41:453–80.
[6] Schumann U. Subgrid-scale model for finite difference simulation of turbulent flows in plane channels and annuli. J Comput Phys 1975;18:376–404.
[7] Moin P, Kim J. Numerical investigation of turbulent channel flow. J Fluid Mech 1982;118:341–77.
[8] Piomelli U, Ferziger JH, Moin P, Kim J. New approximate boundary conditions for large eddy simulations of wall-bounded flows. Phys Fluids A 1989;1:1061–8.
[9] Hoffman G, Benocci C. Approximate wall boundary conditions for large-eddy simulations. In: Benzi R, editor. Advances in turbulence V. Dordrecht: Kluwer Academic Publishers; 1995. p. 222–8.
[10] Wang M, Moin P. Dynamic wall modeling for large-eddy simulation of complex turbulent flows. Phys Fluids 2002;14:2043–51.
[11] Balaras E, Benocci C. Subgrid-scale models in finite-difference simulations of complex wall bounded flows. In: AGARD CP 551, AGARD, Neuilly-sur-Seine, France, 1994. p. 2.1–5.
[12] Balaras E, Benocci C, Piomelli U. Two layer approximate boundary conditions for large-eddy simulations. AIAA J 1996;34:1111–9.
[13] Cabot WH. Large-eddy simulations with wall models. In: Annual research briefs—1995, Center for Turbulence Research, Stanford University, Stanford, CA, 1995. p. 41–50.
[14] Cabot WH. Near-wall models in large-eddy simulations of flow behind a backward-facing step. In: Annual research briefs—1996, Center for Turbulence Research, Stanford University, Stanford, CA, 1996. p. 199–210.
[15] Cabot WH, Moin P. Approximate wall boundary conditions in the large-eddy simulation of high Reynolds number flows. Flow Turb Combust 2000;63:269–91.
[16] Kemenov KA, Menon S. Explicit small-scale velocity simulation for high-*Re* turbulent flows. J Comput Phys 2006;220:290–311.
[17] Kemenov KA, Menon S. Explicit small-scale velocity simulation for high-*Re* turbulent flows. Part II: non-homogeneous flows. J Comput Phys 2007;222:673–701.
[18] Gungor AG, Menon S. Direct simulation of subgrid turbulence in a high-*Re*, wall-bounded flow. AIAA Paper 2006-3538, 2006.
[19] Spalart PR, Jou WH, Strelets MK, Allmaras SR. Comments on the feasibility of LES for wings, and on a hybrid RANS/LES approach. In: Liu C, Liu Z, editors. Advances in DNS/LES. Columbus, OH: Greyden Press; 1997. p. 137–48.
[20] Nikitin NV, Nicoud F, Wasistho B, Squires KD, Spalart PR. An approach to wall modeling in large-eddy simulations. Phys Fluids 2000;12:1629–32.
[21] Baggett JS. On the feasibility of merging LES with RANS in the near-wall region of attached turbulent flows. In: Annual research briefs—1998, Center for Turbulence Research. Stanford, CA: Stanford University; 1998. p. 267–77.
[22] Piomelli U, Balaras E, Pasinato H, Squires KD, Spalart PR. The inner-outer layer interface in large-eddy simulations with wall-layer models. Int J Heat Fluid Flow 2003;24:538–50.
[23] Keating A, Piomelli U. A dynamic stochastic forcing method as a wall-layer model for large-eddy simulation. J Turbul 2006;7(12):1–24.
[24] Radhakrishnan S, Piomelli U, Keating A, Silva Lopes A. Reynolds-averaged and large-eddy simulations of turbulent non-equilibrium flows. J Turbul 2006;7(63):1–30.

[25] Hamba F. A hybrid RANS/LES simulation of turbulent channel flow. Theor Comput Fluid Dyn 2003;16:387–403.
[26] Hamba F. A hybrid RANS/LES simulation of high-Reynolds-number channel flow using additional filtering at the interface. Theor Comput Fluid Dyn 2006;20:89–101.
[27] Temmerman L, Hadziabdic M, Leschziner MA, Hanjalic K. A hybrid two-layer URANS-LES approach for large eddy simulation at high Reynolds numbers. Int J Heat Fluid Flow 2005;26:173–90.
[28] Davidson L, Peng S. Hybrid LES-RANS modelling: a one equation SGS model combined with a $k-\omega$ model for predicting recirculating flows. Int J Numer Meth Fuids 2003;43:1003–18.
[29] Yoshizawa A. Bridging between eddy-viscosity-type and second-order turbulence models through a two-scale turbulence theory. Phys Rev E 1993; 48(1):273–81.
[30] Davidson L. Hybrid LES-RANS: inlet boundary conditions. In: Skallerud B, Andersson H, editors. Third national conference on computational mechanics—MekIT'05; 2005. p. 7–22.
[31] Baurle RA, Tam C-J, Edwards JR, Hassan HA. Hybrid simulation approach for cavity flows: blending, algorithm, and boundary treatment issues. AIAA J 2003;41(8):1463–80.
[32] Xiao X, Edwards JR, Hassan HA. Blending functions in hybrid large-eddy/Reynolds-averaged Navier–Stokes simulations. AIAA J 2004;42(12):2508–15.
[33] Edwards JR, Choi J-I, Boles JA. Hybrid LES/RANS simulation of a Mach 5 compression—corner interaction. AIAA Paper 2008-0718, 2008.
[34] Menter FR. Two equation eddy viscosity turbulence models for engineering applications. AIAA J 1994;32(8):1598–605.
[35] Jiménez J, Pinelli A. The autonomous cycle of near-wall turbulence. J Fluid Mech 1999;389:335–59.
[36] Pope SB. Turbulent flows. Cambridge, UK: Cambridge University Press; 2000.
[37] Grötzbach G. Direct numerical and large eddy simulations of turbulent channel flows. In: Chereminisoff NP, editors, Encyclopedia of fluid mechanics, vol. 6, Gulf, 1987. p. 1337–91.
[38] Marusic I, Kunkel GJ, Porté-Agel F. Experimental study of wall boundary conditions for large-eddy simulation. J Fluid Mech 2001;446:309–20.
[39] Mason PJ, Callen NS. On the magnitude of the subgrid-scale eddy coefficient in large-eddy simulations of turbulent channel flow. J Fluid Mech 1986; 162:439–62.
[40] Wu X, Squires KD. Prediction of the three-dimensional turbulent boundary layer over a swept bump. AIAA J 1998;36(4):505–14.
[41] Wang M. LES with wall models for trailing edge aeroacoustics. In: Annual research briefs—1999, Center for Turbulence Research, Stanford University, Stanford, CA, 1999. p. 355–64.
[42] Werner H, Wengle H. Large-eddy simulation of turbulent flow around a cube in a plane channel. In: Durst F, Friedrich R, Launder BE, Schumann U, Whitelaw JH, editors. Selected papers from the 8th symposium on turbulent shear flows. New York: Springer; 1993. p. 155–68.
[43] Moeng CH. A large-eddy simulation model for the study of planetary boundary-layer turbulence. J Atmos Sci 1984;41:2052–62.
[44] Radhakrishnan S, Keating A, Piomelli U, Silva Lopes A. Large-eddy simulations of high Reynolds-number flow over a contoured ramp. AIAA Paper 2006-899, 2006.
[45] Radhakrishnan S. Large-eddy simulation of high Reynolds-number flows in complex geometries. PhD thesis, University of Maryland, College Park, MD, December 2007.
[46] Song S, Eaton JK. Reynolds number effects on a turbulent boundary layer with separation, reattachment, and recovery. Exp Fluids 2004;36:246–58.
[47] Spalart P, Allmaras S. A one-equation turbulence model for aerodynamic flows. La Rech Aérosp 1994;1:5–21.
[48] Radhakrishnan S, Piomelli U. Large-eddy simulation of oscillating boundary layers: model comparison and validation. J Geophys Res 2008;113(C02022): 1–14.
[49] Meneveau C, Lund TS, Cabot WH. A Lagrangian dynamic subgrid-scale model of turbulence. J Fluid Mech 1996;319:353–85.
[50] Jensen BL, Sumer BM, Fredsøe J. Turbulent oscillatory boundary layers at high Reynolds numbers. J Fluid Mech 1989;206:265–97.
[51] Hunt JCR, Wray AA, Moin P. Eddies, streams, and convergence zones in turbulent flows. In: Studying turbulence using numerical simulation databases, vol. 2. Proceedings of the 1988 summer program, Stanford University, 1988. p. 193–208.
[52] Dubief Y, Delcayre F. On coherent vortex identification in turbulence. J Turbul 2000;1:1–22.
[53] Robinson SK. Coherent motions in the turbulent boundary layer. Annu Rev Fluid Mech 1991;23(1):601–39.
[54] Wang M, Moin P. Computation of trailing-edge flow and noise using large-eddy simulation. AIAA J 2000;38(12):2201–9.
[55] Diurno GV, Balaras E, Piomelli U. Wall-layer models for LES of separated flows. In: Geurts BJ, editor, Modern simulation strategies for turbulent flows. Philadelphia: R.T. Edwards; 2001. p. 157–74.
[56] Tessicini F, Temmerman L, Leschziner M. Approximate near-wall treatments based on zonal and hybrid RANS–LES methods for LES at high Reynolds numbers. Int J Heat Fluid Flow 2006;27:789–99.
[57] Travin AK, Shur M, Spalart P, Strelets MK. Improvement of delayed detached-eddy simulation for LES with wall modelling. In: Wesseling P, Oñate E, Pèriaux J, editors, European conference on computational fluid dynamics ECCOMAS CFD 2006, TU Delft, 2006. p. 410–32.
[58] Shur ML, Spalart PR, Strelets MK, Travin AK. A hybrid RANS/LES model with delayed DES and wall-modeled LES capabilities. Int J Heat Fluid Flow, 2008, to appear.
[59] Germano M. Properties of the hybrid RANS/LES filter. Theor Comput Fluid Dyn 2004;17(4):225–31.
[60] Sánchez-Rocha M, Kirtaş M, Menon S. Zonal hybrid RANS–LES method for static and oscillating airfoils and wings. AIAA Paper 2006-1256, 2006.
[61] Sánchez-Rocha M, Menon S. The compressible hybrid RANS/LES governing equations. Bull Am Phys Soc 2007;52(12):172.
[62] Rajamani B, Kim J. A numerical simulation of hybrid-filtered Navier–Stokes equations. Bull Am Phys Soc 2007;52(12):172.
[63] Nicoud F, Baggett JS, Moin P, Cabot WH. Large eddy simulation wall-modeling based on suboptimal control theory and linear stochastic estimation. Phys Fluids 2001;13:2968–84.
[64] Porté-Agel F, Meneveau C, Parlange MB. A scale-dependent dynamic model for large-eddy simulation: application to a neutral atmospheric boundary layer. J Fluid Mech 2000;415:261–84.